QUANTITATIVE 3D CHARACTERISATION OF THE PORE SPACE OF REAL ROCKS: IMPROVED μ-CT RESOLUTION AND PORE EXTRACTION METHODOLOGY

S. Youssef, E. Rosenberg, N. Gland, S. Bekri, O. Vizika
Institut Français du Pétrole, 1 et 4 avenue de Bois-Préau, 92852 Rueil-Malmaison, France

This paper was prepared for presentation at the International Symposium of the Society of Core Analysts Calgary, September 10-12, 2007

ABSTRACT

Pore network models are generally used to calculate and predict two phase transport properties of porous media from pore space structure information. The predictability of such models depends on the accuracy with which the network captures the complex geometric and topological properties of the pore space. High resolution Computed Micro Tomography (CMT) appears to be the ideal method to validate these models and improve their predictability in the case of complex geometry media.
In this paper, we present a methodology combining high resolution CMT measurement, providing 2000^3 voxel images at micron resolution in less then 3h acquisition time, and a fast and efficient partitioning of the pore space enabling a complete and realistic description of the geometry and topology of the associate large subsets. Relevant parameters are then extracted for pore network simulations. The partitioned volume is directly used to simulate mercury injection which is confronted to experimental HPMI results. The equivalent extracted network is used to calculate absolute permeability using a Pore Network Model (PNM) code. The methodology is applied to a set of real porous media and shows a good agreement between experiments and simulation when the studied volume is representative.

INTRODUCTION

The development of computational methods to analyze the 3D structure of pore networks has known tremendous advance with the advent of Synchrotron CMT (Computed Micro Tomography) generating 3D data sets at the micron scale (Coles et al 1996, Lindquist et al 2000, Knackstedt et al 2004). Fluid transport calculations initially based upon reconstructions from 2D thin sections (Adler et al 1998) or upon numerical reconstructions (Valvatne et al 2003, Oren et al 2006) have been extended to 3D CMT images with the promise to contribute to the improvement of multiphase fluid displacement prediction in porous media. Furthermore, by enabling the direct vizualisation of fluids in the pore network (Seright et al 2005, Prodanovic et al 2006), CMT studies will contribute to a better understanding of trapping mechanisms or changes in flow properties as the pore structure or wettability varies. Highly interdisciplinary teams have contributed to improve topological partitions and fluid transport predictions based on these CMT data (Arns et al 2004, Bauget et al 2005, Knackstedt et al 2006,

Olafuyi et al 2006). Several algorithms exist to extract pore networks from CMT data. They can be roughly classified in two types: partition of the pore space using pore bodies and throat detection like proposed by Lindquist et al (2000) and Knackstedt et al (2004), and partition of the grain (Thompson et al 2005, Sheppard et al 2006), the last being more appropriate for clastic rocks. Emerging laboratory CMT equipments providing resolutions of a few microns give a new invigoration to these methodologies by providing the opportunity to go further in the complexity and representativity of rocks in terms of structure and wettability. In this study we present an integrated methodology for the extraction of pore networks of actual rocks using a high performance lab equipment (acquisition time and resolution), an efficient home made algorithm for partitioning the pore space, the fine control of this partitioning via efficient 3D displays, and via flow calculations (drainage Pc curve, absolute permeability) directly performed on the extracted networks.

EXPERIMENTAL METHODOLOGY

Imaging setup for X-Ray Microtomography

The CMT equipment installed at IFP is a Nanotom from PHOENIX X-Ray (Germany). The source is generated by the impact of a focused electron beam on a thin target. Spot size varies between 1 and 5 microns depending on the operating conditions. The diverging geometry of the X-Ray source results in a magnification of the object image. The detector is a Hamamatsu flat detector (110mm×110mm) made of 2304×2304 pixels, 50 microns size. Generating images using microfocus CT starts with the acquisition of a series of 2D projections while progressively rotating the sample step by step through a full 360° rotation at increments of less than 1°. The entire diameter of the sample should remain within the field of view throughout the entire 360° rotation: a 5mm diameter sample will be completely displayed on each projection with a pixel size of 3 microns. To illustrate the resolution performance of our equipment a test was performed on a foam sample made of empty glass beads with a 2 micron wall thickness in a resin matrix. This is a perfect sample to test 3D resolution while taking into account the whole acquisition-reconstruction chain. The gray level profile shown on **Figure 1** attests for a resolution better than 2 microns.

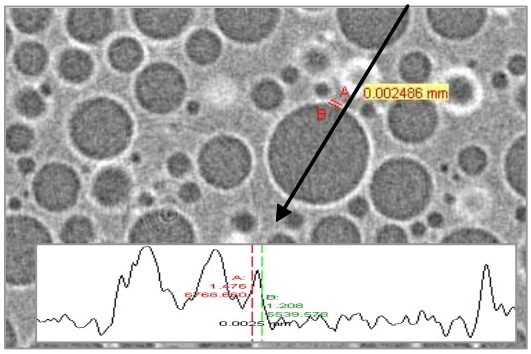

Figure 1: Resolution test on a foam made of 2 micron thick empty glass beads enbedded in a resin. The intensity profile through glass reference and walls attests for a resolution better than 2 microns.

Acquisition parameters for rock analysis were the following: 5mm diameter sample, source object distance 12mm, source-detector distance 200mm, pixel size 3 microns, 2000×2000 field of view, 90KV, 170µA, 0.2° angular step, Cu 0.1mm filter, 2h30

acquisition time. Each acquisition generates 1800 TIFF projections coded in 12 bits (about 10Mo each) which represents about 18 Go per data set. These data sets are used for the numerical reconstruction of the volumetric data.

Reconstruction

The reconstruction (PHOENIX algorithm) uses a classical cone beam Feldkamp algorithm. CMT images are corrected from beam hardening effect both by using a metal filter (Cu) and by using a mathematical correction during the reconstruction process (Phoenix).

High resolution CMT images are also often corrupted by the so called ring artefacts. Particularly when CMT systems are pushed to the extremes in the quest for the ultimate spatial resolution, ring artefacts caused by heterogeneities of the detector elements response can hardly be avoided. In the operating conditions used, these rings are reduced and do not affect the further treatment. They have not been corrected.

Reconstructions are performed in 16 bits on a 4-fold PC cluster of 64bit dual core CPU. The maximum unit volume which can be reconstructed at full resolution is 1000×1000×500 (about 25 minutes reconstruction). For each sample, two consecutive high resolution volumes 1000×1000×500 are reconstructed and appended to form the basic 1000×1000×1000 volume on which the treatment will be done. Subset volumes can then be extracted from this 1000×1000×1000 basic volume. In order to reduce their disc size and allow bigger volume access, the volumes can be converted into a 8 bit format or/and binned if we need not the full resolution.

PORE NETWORK EXTRACTION METHODOLOGY

The objective is to capture the resolved pore space (size higher than the resolution), partition it into pore bodies, pore throats and channels and describe their connections. This treatment consists in four main steps: binarisation, skeleton extraction, pore space partitioning and parameters extraction.

Binarisation

The first step is a binarisation of the gray level image to isolate the resolved porosity. The procedure applied to get the final binary image of the pore space is the following: thresholding at a convenient gray level (defined below) between the two peaks; smoothing the selected region; removing of 3D islands more than 2000 pixels in the selected pore volume and finally removing the unconnected region on the negative 3D image (mineral phase). The resolved porosity (macroporosity) is evaluated as the percentage of selected voxels at the local interpeak minimum. The threshold is chosen a few units above the minimum in order to recover this macroporosity after the smoothing and island removing treatment. In practice, this threshold corresponds to a percentage of selected voxels 10% (relative) higher than the reference porosity (see **Figure 2**).

Skeleton extraction

The skeleton extraction algorithm has initially been developed at INRIA for micro-vascular network analysis (Fouard et al 2004, Cassot et al 2006) and integrated into the

commercial Amira software. It is based on a hybrid algorithm that combines thinning and distance map based techniques called *Distance Ordered Homotopic Thinning*. This algorithm computes the shortest distance of each point of the foreground (void space) to the background using chamfer methods. The resulting distance map is used to guide the thinning algorithm. Finally the distance map is used to mark each voxel of the skeleton with the minimum distance to the boundary of the void space.

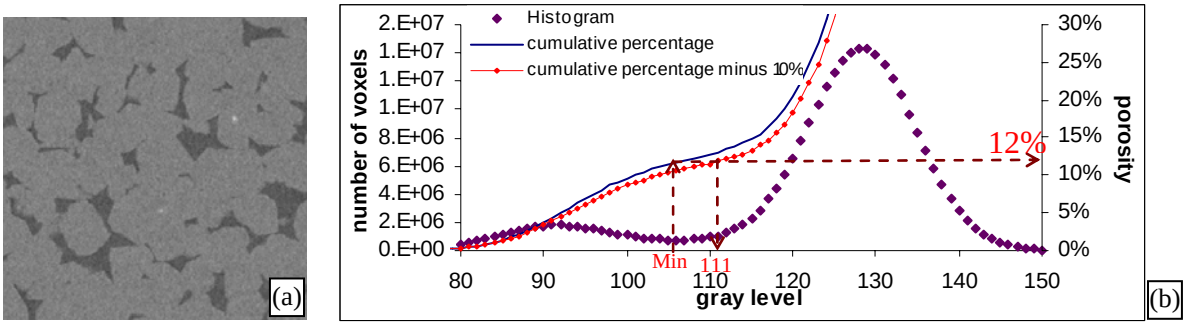

Figure 2 (a) X-Ray density maps of a Fontainebleau sample. (b) Histogram of gray levels: Frequency (left axis) and cumulated percentage (right axis) of selected voxels (c) Segmented image obtained by thresholding at the local interpeak minimum (106). (d) Segmented image obtained by thresholding at the defined gray level (111) followed by a smoothing and small islands elimination. Segmented images (c) and (d) have respectively a porosity of 12.4% and 12.3%.

Pore space partitioning

The algorithm used in this part of the treatment has been developed at IFP in C++ and can be added as "home made" modules of Amira. The usual conceptual representation of PNM divides the void space into nodal pores connected by channels containing throats. This algorithm uses the skeleton network marked with the corresponding minimal diameters as an embedded search structure operating in the segmented image to find the restrictions or throats of the network. As it is shown on **Figure 3** a channel is generally described by a single line while the pores, on the contrary are described by a group of lines and vertices. The algorithm is conducted in three main steps as shown on **Figure 3**.

The aim of the first step is to identify the lines describing exclusively the channels and to find the corresponding throat points (cf. **Figure 3b**). Each line is represented by a set of connected voxels and the connectivies of a line are equal to the connectivity of its two ends voxels (**Figure 4**). For each line we determine the connectivity numbers and the label of the neighboring lines at both ends. Then, a cleaning operation is undertaken in which all dead ends (one end with connectivity 1) and loop lines (same voxel for the two ends) are eliminated. The resulting neighbor lines with a connectivity "2" are merged in one single line. Once the skeleton is cleaned, we calculate the length of each line. If the length of a line is lower than one of its extremity radius the line is classified as a pore

line. Finally, we search for the minimum radius on each channel line. At this step, we calculate channel lengths and their hydraulic radii.

The goal of the second step is to partition the skeleton into groups of lines belonging to the same pore (cf. **Figure 3c**). This objective is reached in three steps. First the skeleton is stored in a table as a binary image where the value of the skeleton voxels is 1 and the background is 0. Then, each voxel corresponding to a throat is turned into a zero value. This operation produces separated groups of connected lines (clusters) belonging to the same pore. Finally, each cluster is given a different gray value. The image is coded in unsigned 16 bits allowing the differentiation of 65535 clusters. Once the clusters are labeled, a search algorithm detects the maxima distance for each cluster. This distance corresponds to the maximal embedded sphere radius in the pore.

In the third step the geometrical separation and labeling of pores is done by adding the binary image of the void space to the labeled cluster image. Then using a voxel growth constrained algorithm, the labeled pore space is reconstructed and pores are automatically separated. The partitioned volume can be visualized to control the partitioning efficiency.

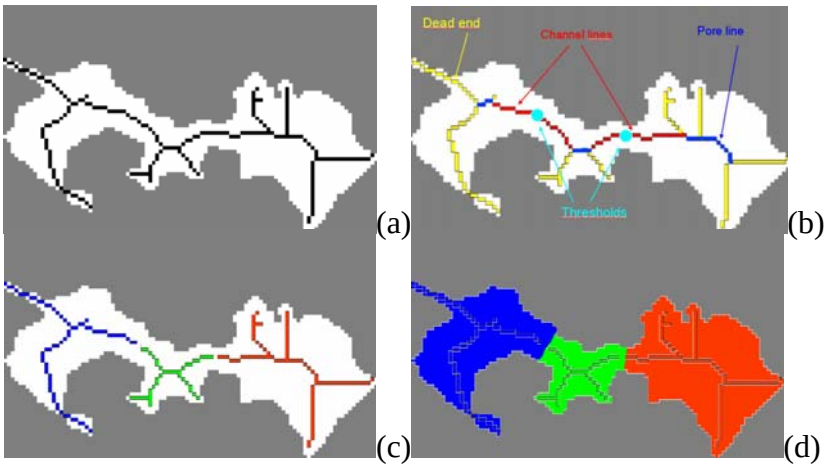

Figure 3 (a) Initial skeleton of the pore space, (b) Identifying channel lines (red), pore lines (blue) and dead ends (yellow), (c) Identifying throats in the channels lines (minimum diameter) and labelled pore segments (d) Reconstruction of labelled pores for pore volume estimation

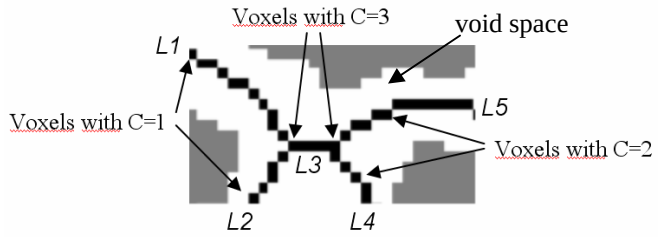

Figure 4 2D illustration of an embedded skeleton with 5 lines (L1 to L5). The connectivity of each line corresponds to the connectivity C of its ends voxels.

Parameters extraction

Parameters to be used in the PNM code are extracted from the 3D pore space images.

- pore-throat radii: the pore-throats are the pore restrictions. The minimum radius of each throat is known. The cross section area at the throat location is used to calculate the shape factor and the equivalent radius r_{eq} assuming an elliptic section.
- coordination number: is the number of pores connected to a given pore.
- pore radii: a pore is defined as a porous volume closed by restrictions. Its volume is measured from the partitioned image of the pore space. Its radius is defined as the radius

of the equivalent sphere having the same volume. The radius of the maximum ball included in this volume is also calculated.
- throat length: pore network models use channels with a constant diameter. In real rocks, this diameter is not constant. A real channel (**Figure 5**) can be represented by a series of elementary cylinders of variable and known radii r_i and of equal (one voxel) thickness.

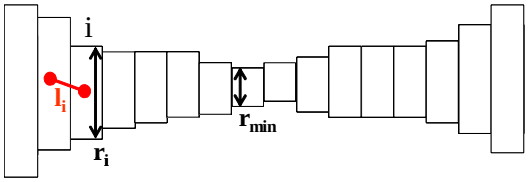

Figure 5 Schematic representation of a real channel.

The fluid conductance of an elementary cylinder *i* is defined by : $g_i = \frac{\prod r_i^4}{8\mu l_i}$

The conductance g_{eq} of the equivalent cylindrical tube of radius r_{min} is defined by $\frac{1}{g_{eq}} = \Sigma \frac{1}{g_i} = \frac{8\mu}{\pi} \sum_{i=1}^{n} \frac{l_i}{r_i^4} = \frac{8\mu l_{eq}}{\pi \cdot r_{min}^4}$. The length of the equivalent cylindrical tube is then given by: $l_{eq}^n = \sum_{i=1}^{n_{max}} l_i \left(\frac{r_{min}}{r_i} \right)^4$ where n_{max} is the number of elements in the real channel line. This length l_{eq} may be very different from the actual channel length from one pore to the other.

SIMULATIONS

Mercury intrusion simulation

Once the partitioning is done, a connection matrix is built from which mercury porosimetry can be simulated. Throat sizes are stored in a array in which the line number I and the column number J correspond to the pore numbers linked to the throat (I, J). To begin the mercury intrusion simulation, the volume is supposed to be surrounded by mercury and the edge pores are supposed to be already full with mercury. At a fixed capillary pressure, all the pores connected to an already invaded pore via a throat greater than or equal to the equivalent pore entry radius are invaded. Decreasing the throat radius, the non wetting phase saturation is calculated from the total volume of invaded pores. The applied pressure is assumed to be inversely proportional to the diameter via Laplace equation.

In the experimental mercury invasion test, the invaded volume is expressed relative to the total pore volume. In order to compare simulated and experimental curves we must know the total pore volume including the micro porosity (not resolved with CMT). In a mono-mineral matrix, the global porosity can be deduced from the mean grey level (L_{mean}) of the 3D volume defined as $L_{mean} = \sum_{i=1}^{N} N_i L_i / \sum_{i=1}^{N} N_i$ (N_i number of voxels with L_i gray level) and the min and max grey level values measured respectively on the voids (L_{void}) and on the solid phase (L_{solid}). Global porosity is given by : $P=(L_{solid}-L_{mean})/(L_{solid}-L_{void})$. This estimation requires a good beam hardening correction. In macroporous samples like

Fontainebleau sandstones, these min and max values are the abscissa of the two maximum peaks in the histogram.

Permeability calculation

Absolute permeability calculation is performed directly on the extracted numerical network. The simulation uses the pore size and coordinates, throat size and channels length between these pores and their neighbours. The principle of permeability calculation is the same as for a regular network and has been reported previously (Laroche et al 2001).

RESULTS AND DISCUSSION

The procedure has been applied on both sandstones and limestones. We present here the results obtained on a suite of four Fontainebleau samples and on two limestone (Estaillades and Brauvilliers) samples.

Fontainebleau sandstones

The Fontainebleau sandstones suite provides the ideal experimental system to test the whole procedure since a considerable amount of data is available from both the petrophysical and microtomography points of view (Bourbié et al 1985, Lindquist et al 2000, Sok et al 2004). Moreover, the geological uniformity of Fontainebleau sandstones gives an exceptional quality to the permeability-porosity relationship which can be used as a reference.

The approach described in the previous paragraph is applied to a subset of 500x500x500 voxels reconstructed with half resolution (6 microns resolution) and when necessary the same method is applied to a smaller subset of 500x500x500 voxels reconstructed with 3 micron resolution. A selection of the X-Ray density map of four Fontainebleau samples (6 micron resolution) is given in **Figure 6.** Differences between the plugs are immediately obvious: the solid phase is identical in all the samples (quartz grain size approximately 250 microns) and the intergranular porosity is reduced from the first to the last sample. The total porosity of the studied subvolumes is directly deduced from the mean grey level value of the histogram taking the two grey level maxima as references. Measured global porosities are respectively 21.6%, 14.2%, 12.3% and 6.5%.
The different steps of the pore network extraction are illustrated in 3D on the 12% porosity Fontainebleau sample (**Figure 7**). **Figure 8** is a zoomed view of the partitioned volume on a small part of the volume.

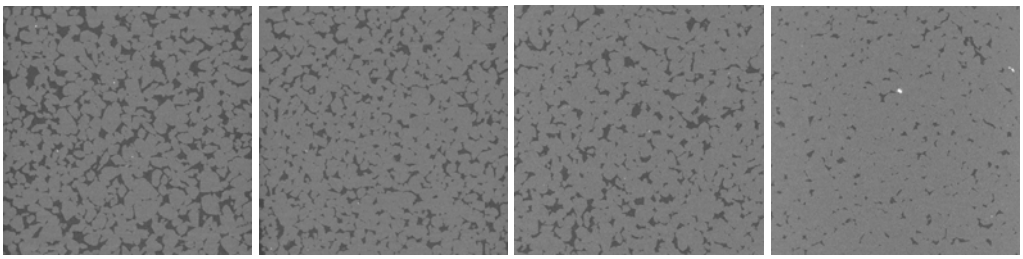

Figure 6 X-Ray density maps of four Fontainebleau samples extracted from 500^3 voxel volumes at 6 micron resolution with porosities from left to right of 21.6%, 14.2%, 12.3% and 6.5%.

Each pore is represented with a different colour in order to appreciate visually the partitioning quality. Amira software used for this 3D visualisation also enables to control the throat surfaces (patches) between two adjacent pores. Efficiency of the treatment can thus be controlled at this step for all the subsets. In our methodology, the drainage Pc curve is obtained by invading step by step the whole volume accessible via the throat radius corresponding to a fixed capillary pressure. The curves are compared to a mercury invasion experiment conducted on a sister plug of each sample. In the experimental mercury invasion test, the invaded volume is expressed relative to the total pore volume. In CMT simulations, the invaded volume is expressed relative to the total pore volume measured on the image block. The matching of experiments (**Figure 9**) is satisfactory in all cases for high porosity samples. For the lowest porosity sample, the best fit is obtained with a 3 µm resolution without performing any smoothing. The permeability calculations have been performed on all 500^3 voxel subset volumes with 6 micron resolution. All the simulated points are fitting the reference permeability versus porosity curve (Zinszner 2007) except

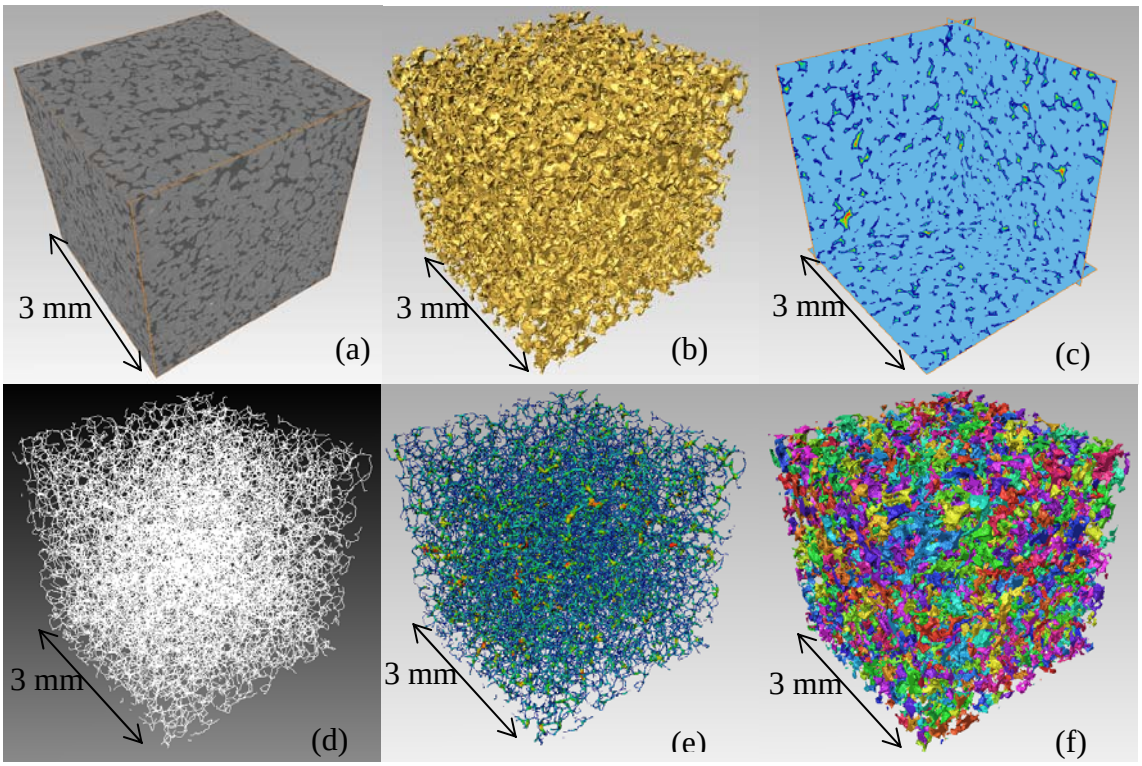

Figure 7 3D view of the six main steps of the treatment : acquisition of a 3D block (a), isolating the porosity by binarisation (b), computing the 3D distance map(c), extracting the skeleton (d) marked with minimum distance to the border in each point (e),and partitioning the pore space into individual pores (f).

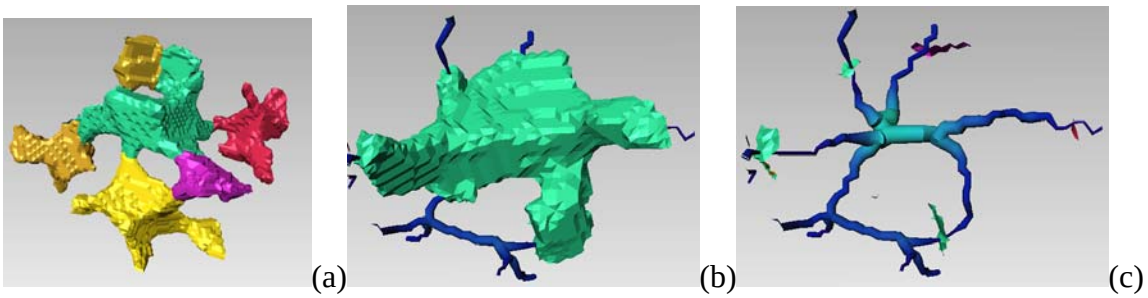

Figure 8 : Zoomed view of the partitioned volume: (a) Six pores are represented with a different colour (b) Detail of one pore and its connections (c) Representation of the throat surfaces at connections.

for the lowest porosity sample. For this sample, at 6 µm resolution, the pore network is not represented by a single and continuous cluster but by several clusters among which very few are percolating which explain the low permeability (0.3 mD). At 3 µm resolution we recover a single percolation cluster and we obtain 18 mD of permeability which is more realistic. The influence of the smoothing treatment seems almost negligible (18mD and 29 mD respectively with and without a smoothing treatment).

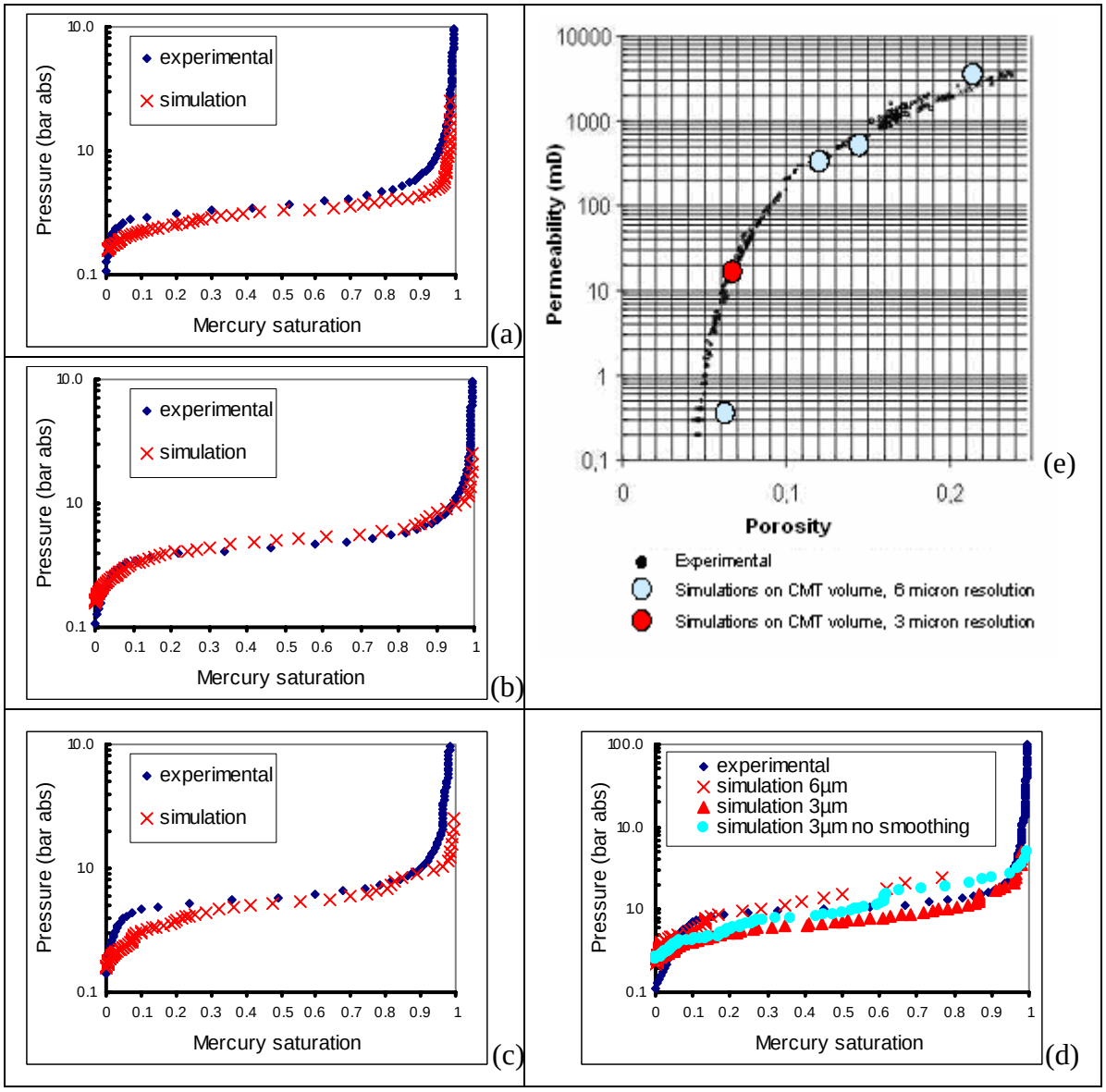

Figure 9 : Simulation results on Fontainebleau sandstone samples : (a) to (d) : Mercury intrusion simulation and experiments on samples A to D (e) : Permeability simulations and experiments

Carbonate samples

Estaillades and Brauvilliers are vuggy carbonates presenting similar drainage behaviour and comparable capillary pressure curves but very distinct imbibition behaviour (Moctezuma et al 2002, Han et al 2007). Lacking any detailed 3D information about the pore structure, this behaviour was attributed to different 3D structure and connectivity. Computed Micro Tomography gives presently the possibility to verify this initial assumption. Estaillades contains microporous algae (intermediate grey level particles in **Figure 10a**). The binarisation step enables to isolate the macroporous network (**Figure 10b**). In this sample, the macroporosity and microporosity are two independant networks.

The mean porosity (deduced from the mean gray level) is 21% and the macroporosity (deduced from the thresholding described in **Figure 2**) is 14.3%.

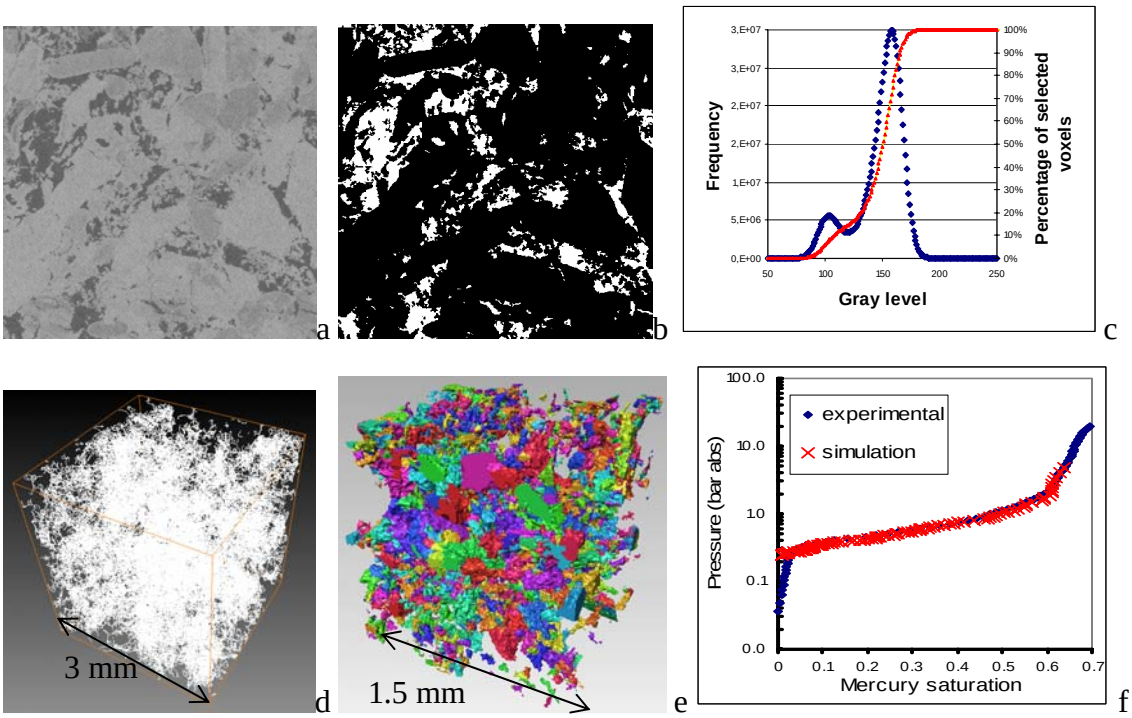

Figure 10 : Results on Estaillades carbonate. (a): 1000^3, 3 micron resolution X-ray density map (b, c) Binarisation step (d) 1000^3 3D skeleton representation (e) 500^3 partitioning of the pore space (f) Mercury intrusion simulation (1000^3volume-3 micron resolution) and experiment.

In spite of a complex skeleton (**Figure 10d**), the resolved porosity appears to be a single percolating cluster and the treatment leads to a satisfying partitioning. The quality of the partitioning can be appreciated visually (**Figure 10e**) and quantitatively via the comparison between simulations and experiments. The fit between experimental and simulated mercury intrusion curves is very satisfactory (**Figure 10f**). The permeability simulation conducted on a 800^3 block with 3 µm resolution, leads to a value of k=80mD while a value of k=130mD is measured on a sister plug (40mm diameter, 80mm long**,** 25% porosity).

Brauvilliers sample has a very different texture. It contains oolithes and the intra-oolithic macroporosity is accessible either via the microporous cortex or via macropores. An intergranular macroporosity is clearly visible on the 2D sections (**Figure 11a**). The mean porosity (deduced from the mean gray level) is 22.6% and the macroporosity (deduced from the thresholding described in Figure 2) is 16.8%. These values are far below the porosity measured on a 40mm sister plug (32%) but this difference can be attributed to the heterogeneous distribution of porosity in this sample : the CMT image of this 40mm plug rescaled with a 3mm pixel size (equivalent to our subset volume) shows a variability of porosity values from 18 to 38%. This example demonstrates the limitations of the use of CMT to obtain a representative description of fine pore heterogeneous porous media. Even with the best resolution accessible presently, pores smaller than 1micron cannot be

resolved and because of its multi scale heterogeneity, the representative elementary volume cannot always be reached at high resolution. In the studied block, resolved porosity is not represented by a single percolation cluster but by a set of individualized pores and a big cluster (in **Figure 11d**: the cluster is represented in purple). The fit between experimental and simulated mercury intrusion curves is acceptable but only a part of the macroporosity is invaded. The permeability calculation has not been possible because the unique cluster is not percolating from one side to the opposite side. A more complete description taking into account both the heterogeneity at higher scale (determined by CMT) and the microporosity contribution (evaluated by a global approach Bekri et al 2005) will be necessary to get reliable properties on such a sample.

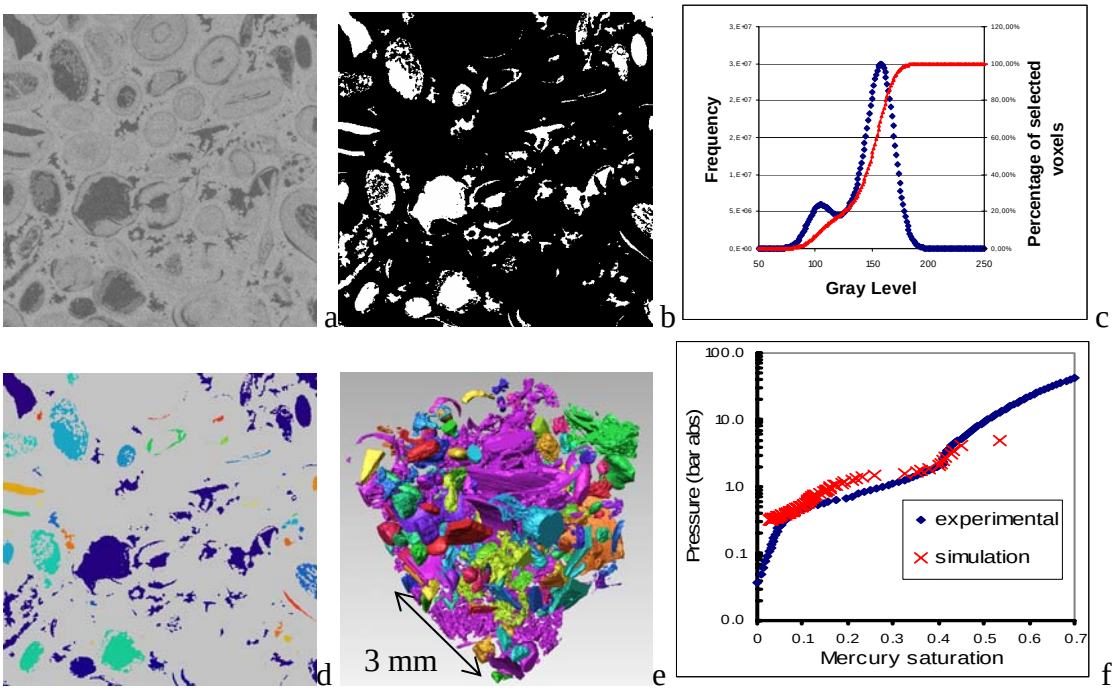

Figure 11: Results on Brauvillier carbonate. (a): 1000^3, 3 micron resolution density map (b, c) Binarisation step. The binarisation do not lead to a single cluster: (d) connected pores are represented in dark blue (e) 1000^3 3D representation of the individual clusters: none of them is percolating (f) 1000^3 mercury intrusion simulation and experiment

CONCLUSIONS

In this paper, we present a methodology combining a high resolution CMT laboratory analysis and an efficient partitioning of the pore space, enabling a complete and realistic description of the geometry and topology of the pore network.

The methodology has been applied to sandstones and carbonates. A good agreement between experiments and simulations for drainage capillary pressure curve and absolute permeability is obtained as far as the resolved pore space is represented by one single connected cluster. For homogeneous porous media without microporosity this condition seems to guarantee that the numerical pore structure describes the real one in terms of representative elementary volume and critical conductive pore size. In carbonates, because of their multi scale heterogeneity, the representative elementary volume cannot

always be reached at high resolution. The challenge of this methodology will be then to increase the volume size examined numerically by using discrete representations of the pore space at the relevant scale in dual pore networks or by using continuum type upscaling techniques to predict flow properties in multi scale heterogeneous samples. An important part of the porosity will remain unresolved in these low permeability rocks characterized by a large spectrum of pore/throat sizes. In these cases the global approach (inversion of macroscopic properties) for the microscale should be combined to CMT in the larger scales.

REFERENCES

1. Adler, P. M. and Thovert, J. F. , "Real porous media: local geometry and macroscopic properties", Appl. Mech. Rev. Vol 51 (1998) 537-585.
2. Arns, J. Y. , Robins, V. , Shepperd, A. , Sok, R. , Pinczewski, W. V. , Knackstedt, M. A. , "Effect of Network Topology on relative permeability" Transport in Porous Media Vol 55 (2004) 21-46
3. Bauget, F. , Arns, C. H. , Sadatfar, M. , Sheppard, V. , Sok, R. M. , Turner, M. L. , Pinczewski, W. V. , Knackstedt, M. A., SPE 95950 (2005), SPE ATCE , Dallas, USA, 2-12 Oct 2005
4. Bekri, S., Vizika, O., "Pore network modeling of rock transport properties : application to a carbonate"", SCA 2006- 22 (2006) Trondheim, Norway, 12-16 Sept 2006
5. Bekri, S., Laroche, C., Vizika, O., "Pore network models to calculate transport and electrical properties of single or dual-porosity rocks", SCA 2005-35 (2005) Toronto, Canada, 21-25 August 2005
6. Bourbié, T., Zinszner, B., " Hydraulic and acoustic properties as a function of porosity in Fontainebleau sandstones", J. Geophys. Res. Vol 90 (1985) 11524-11532
7. Cassot, F. , Lauwers, F. , Fouard, C. , "Three-Dimensional Computer-Assisted Method for a Quantitative Study of Microvascular Networks of the Humean Cerebral Cortex", Microcirculation, Vol 13 (2006)1-18
8. Coles, M. E. , Hazlett, R. D, Muegge, E. L. , Jones, K. W. , Andrews, B. , Dowd B. , Siddons P. , Peskin,A. ,Spanne P. , "Developments in Synchrotron X-Ray Microtomography with Applications to flow in Porous Media", SPE 36531 (1996) The SPE ATCE, Denver, USA, 6-9 October 1996
9. Fouard, C. , Malandain,G. , Prohaska, S. , Westerhoff, M. , Cassot, F. , Mazel,C. , Asselot, D. , and Marc-Vergnes. J. P. , "Skeletonization by blocks for large datasets: application to brain microcirculation", International Symposium on Biomedical Imaging: From Nano to Macro" (ISBI'04), Arlington, USA, April 2004
10. Knackstedt, M. A. , Arns, C. H. , Limaye, A. , Sakellariou, A. , Senden, T. J. , Sheppard, A. P. , Sok,R. M. , Pinczewski,V. , "Digital core laboratory : Properties of reservoir core derived from 3D images", SPE 87009 (2004), The Asia pacific conference on Integrated Modelling Kuala Lumpur, Malaysia, 29-30 March, 2004.
11. Knackstedt, M. , Arns, C. , Ghous, A. , Sakellariou, A. , Senden, T. , Sheppard, A. , Sok, R. , Averdunk, H. , Pinczewski, W, Padhy, G. and Ioannidis, A. "3D imaging and flow characterization of the pore space of carbonate core samples", SCA 2006-023 (2006), Trondheim, Norway, 12-16 Sept 2006
12. Laroche, C., Vizika, O., Hamon, G., Courtial, R. "Two phase flow properties prediction from small scale data using pore-network modeling", SCA 2001-06 (2001), Monterey, USA, Sept 2001
13. Lindquist,W. B., Venkatarangan, A., Dunsmuir J. and Wong. T. "Pore and throat size distributions measured from synchrotron X-ray tomographic images of Fontainebleau sandstones", J. Geophys. Res. Vol 105 (2000**)** 21508-21528
14. Moctezuma, A., Vizika, O., Adler, P. "Water-oil relative permeability in vugular porous media : experiments and simulations", SCA 2002-06, (2002), Monterey, USA, Sept 2002
15. Olafuyi, A. O. , Sheppard, A. P. , Arns, C. H. , Sok, R. M. , Cinar, Y. , Knackstedt, M. A. , Pinczewsli, W. V. , "Experimental Investigation of Drainage Capillary Pressure Computed from Digitized Tomographic Images", SPE 99897 (2006) SPE/DOE Symposium on improved oil Recovery Tulsa, Oklahoma, USA, 22-26 April 2006.
16. Oren, P. E. , Bakke, S. ,and Rueslatten, H. G. "Digital core laboratory : Rock and flow properties derived from computer generated rocks ", SCA 2006-021 (2006), Trondheim, Norway 12-16 September 2006
17. Phoenix X-Ray http://www.phoenix-xray.com
18. Prodanovic, M. , Lindquist, W. B. , Seright, R. S. , "Porous structure and fluid partitioning in polyethylene cores from 3D X-ray microtomographic imaging", J. Colloid and Interface Sci. Vol 298 (2006) 282-297
19. Seright R. S. , Prodanovic, M. , Lindquist W. B. " XRay Computed Microtomography Studies of Fluid partitioning in Drainage and Imbibition before and after gel placement : disproportionate Permeability reduction", SPE 89393 (2005)
20. Sheppard, A. P. , Sok, R. M. , Averdunk, H. , Robins, V. , and Ghous, A. "Analysis of rock microstrcture using high-resolution X-Ray tomography", SCA 2006-026 (2006) Trondheim, Norway 12-16 september 2006
21. Sok, R. M., Knackstedt, M. A. , Sheppard, A. P. , Pinczewski, W.V. , Lindquist, W.B. , Venkatarangan, A. and Paterson, L. "Direct and Stochastic Generation of Network Models from Tomographic Images; Effect of Topology on Residual Saturations", Transport In Porous Media, Vol 46 (2002) 345-372
22. Thompson, K. E. , Willson,C. S. , White,C. D. , Nyman,S. , Bhatttacharya,J. , Reed,A. H. , "Application of a New Grain-Based Reconstruction Algorithm to Microtomography Images for Quantitative characterization and Flow Modeling", SPE 95887 (2005), SPE ATCE , Dallas, Texas, 9-12 October 2005.
23. Valvatne, H. , Blunt, M. "Predictive Pore scale Network modelling", SPE 84550 (2003) SPE ATCE Denver, Col
24. Han, M. , Fleury, M. , Levitz P. "Effect of the pore structure on resistivity index ", SCA (2007) Calgary, Canada.10-13 September 2007